Enhanced extreme ultraviolet high-harmonic generation from chromium-doped magnesium oxide

V E Nefedova, S Fröhlich, F Navarrete, N Tancogne-Dejean, D Franz, A Hamdou, S Kaassamani, D Gauthier, R Nicolas, G Jargot, et al.

,

Enhanced extreme ultraviolet high-harmonic generation from chromium-doped magnesium oxide

V. E. Nefedova,[1] S. Fröhlich,[1] F. Navarrete,[2,3] N. Tancogne-Dejean,[4] D. Franz,[1] A. Hamdou,[1] S. Kaassamani,[1] D. Gauthier,[1] R. Nicolas,[1,5] G. Jargot,[6,7] M. Hanna,[6] P. Georges,[6] M. F. Ciappina,[8,9,10] U. Thumm,[2,a)] W. Boutu,[1] and H. Merdji[1,b)]

[1)]*Ultrafast Nanophotonics group, LIDYL, CEA-CNRS-Université Paris-Saclay 91191, Gif-sur-Yvette, France*

[2)]*Department of Physics, Kansas State University, Manhattan, KS 66506, USA*

[3)]*Institute of Physics, University of Rostock, 18051 Rostock, Germany*

[4)]*Max Planck Institute for the Structure and Dynamics of Matter and Center for Free-Electron Laser Science, Luruper Chaussee 149, 22761 Hamburg, Germany*

[5)]*Department of Natural Sciences, Lebanese American University, 1102 Beirut, Lebanon*

[6)]*Université Paris-Saclay, Institut d'Optique Graduate School, CNRS, Laboratoire Charles Fabry, 91127, Palaiseau, France*

[7)]*Fastlite, 06600 Antibes, Sophia Antipolis, France*

[8)]*ICFO-Institut de Ciences Fotoniques, The Barcelona Institute of Science and Technology, Avenue Carl Friedrich Gauss 3, 08860 Castelldefels (Barcelona), Spain*

[9)]*Physics Program, Guangdong Technion – Israel Institute of Technology, Shantou, Guangdong 515063, China*

[10)]*Technion – Israel Institute of Technology, Haifa, 32000, Israel*

(Dated: 4 April 2021)

High-order harmonic generation (HHG) from crystals is emerging as a new ultrashort source of coherent extreme ultraviolet (XUV) light. Doping the crystal structure can offer a new way to control the source properties. Here, we present a study of HHG enhancement in the XUV spectral region from an ionic crystal, using dopant-induced vacancy defects, driven by a laser centred at a wavelength of 1.55 μm. Our numerical simulations based on solutions of the semiconductor Bloch equations and density-functional theory are supported by our experimental observations and demonstrate an increase of the XUV high harmonic yield from doped bulk magnesium oxide (MgO) compared to undoped MgO, even at low defect concentration. The anisotropy of the harmonic emission as a function of the laser polarization shows that the pristine crystal's symmetry is preserved. Our study paves the way towards the control of HHG in solids with complex defects caused by transition-metal doping.

The interaction of an electric field in the strong field regime with a semiconductor or a dielectric generates electron-hole pairs, which are subsequently accelerated by this field and emit coherent radiation via inter- and intra-band electronic transitions in the solid [1–4]. This coherent emission occurs as bursts of attosecond pulses that have been observed as a harmonic comb in the frequency domain. Since its first experimental observation[5], considerable efforts were devoted to the understanding of the main mechanisms behind high-order harmonic generation in solids (HHG). This new source of extreme ultraviolet (XUV) radiation[6,7] displays a high degree of coherence[8], for instance, suitable for lensless diffractive imaging[9]. It recently provided beams carrying orbital angular momentum with a selective topological charge[10]. Recent studies also reveal that the HHG spatio-temporal properties are intricate due to the complex light-driven electronic dynamics inside the solid. Hence, as a basic application, HHG can reveal information about the crystal's electronic band structure and intrinsic crystal properties[4,11]. Future applications will exploit the ability to manipulate the light-driven electron motion during the crystal HHG process to create optoelectronic devices operating at petahertz frequencies[12–14] or to encode topological information[15]. However, increasing the yield is a prerequisite for the development of a solid state HHG source and its applications. Various experimental techniques, such as plasmon-[16,17], waveguide-[9,18,19] and antenna-enchanced HHG[20], were already implemented to achieve this goal. Here, we propose an alternative way of boosting the HHG yield from solids based on defects. This approach exploits the modification and control of the active medium's electronic structure to tailor the high-order harmonic output signal. Since defects are a corner stone of most modern electronic devices, it appears promising to investigate their influence on the HHG yield. The addition of dopants creates electronic states in the band gap, leading to modifications of the electronic band structure[21,22] and band gaps[23–26], allowing additional optical transitions [27]. Another significant effect of the doping is the appearance of point defects such as vacancies and interstitial sites[28,29]. According to recent theoretical investigations dopant-induced band-gap changes can substantially influence the HHG process[29–33]. In particular, donor-doped materials were theoretically predicted to enhance the HHG yield due to electronic excitation from impurity states[31,33].

a)Corresponding author, email address: thumm@phys.ksu.edu

b)Corresponding author, email address: hamed.merdji@cea.fr

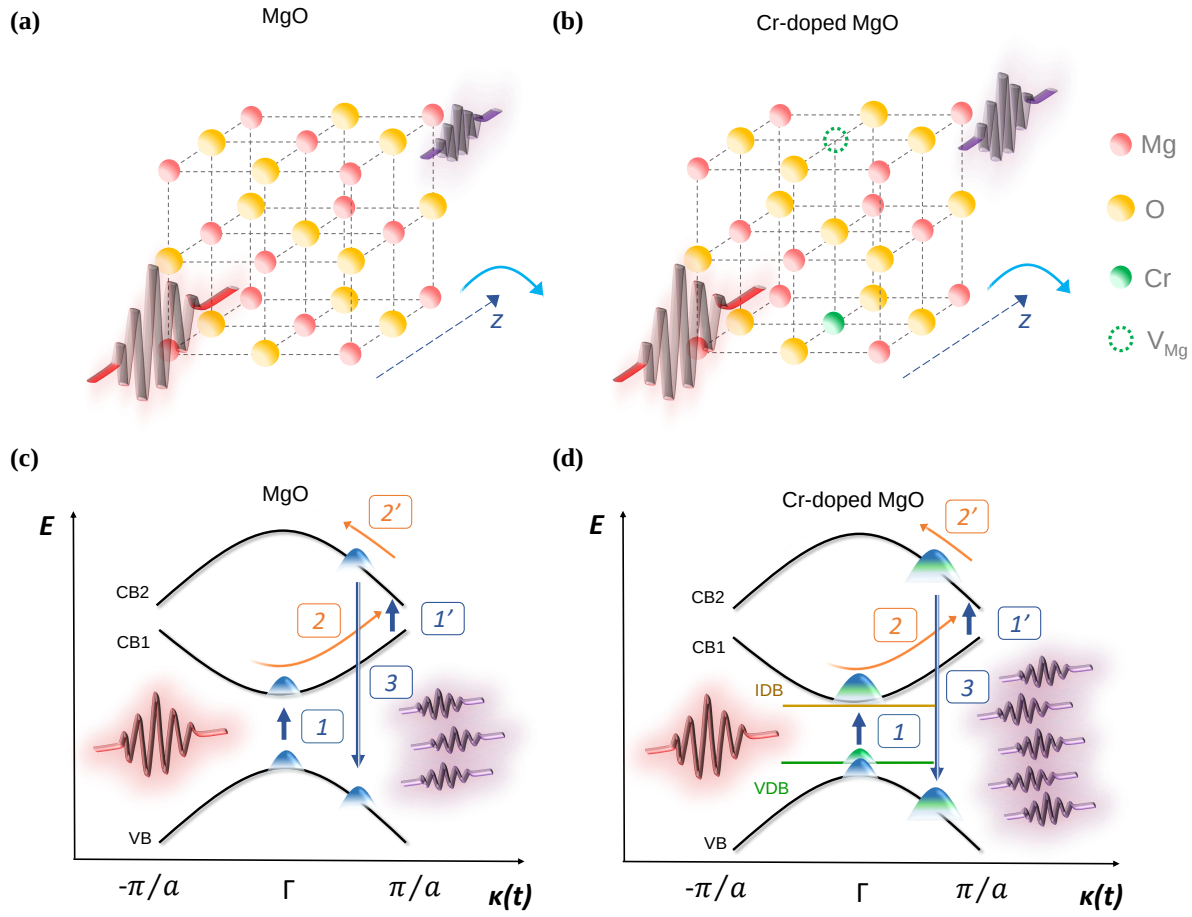

FIG. 1: Schematic of HHG in (a,c) MgO and (b,d) MgO:Cr in (a,b) coordinate and (c,d) momentum space. In (a, b) the laser propagation axis is indicated as z, around which crystals are rotated (light blue arrow) during anisotropy measurements [cf. Figs. 4 (a) and 4 (b)]. (b) A Mg vacancy replaces the closest Mg^{2+} ion along the [100] (C_{4v} symmetry) or [110] direction (C_{2v} symmetry). Both C_{4v} and C_{2v} centers are observed experimentally[27,34]. (c,d) The laser electric field excites an electron wave packet from the valence band (VB) to the first conduction band (CB1) (1, blue arrow), where it experiences intra-band acceleration (2, orange arrow). At higher driver intensities, excitation to (1', blue arrow) and acceleration in (2', orange arrow) higher conductions bands (here CB2) can occur. The excited electron wave packet de-excites to the VB upon recombination with its residual hole (3, blue arrow), emitting harmonics of energy equal to the instantaneous gap in the first BZ. (d) In MgO:Cr the occupied impurity defect band (IDB) and vacancy defect band (VDB) account for additional electronic transitions that enhance the net high-harmonic yield relative to MgO.

We here investigate the influence of dopant-induced vacancies on the HHG yield in chromium-doped magnesium oxide (MgO:Cr), which was extensively studied previously using experimental[34–37] and numerical[38–40] methods. The Cr donor-dopants were found to not only substitute atoms with Cr^{3+} ions in the MgO lattice providing additional electrons, but also to cause the formation of vacancies[34–37] in order to maintain charge neutrality[37].

The HHG process in gases is well explained by the semi-classical "three-step model"[41–43]. A similar approach has been proposed in crystals, where a strong laser electric field generates electron-hole pairs, which are subsequently accelerated by this field and emit radiation via inter- and intraband opto-electronic transitions in the solid[1–4]. The competition between those two mechanisms depends on the material and the driving laser parameters and, as a general feature, intra-band emission dominates at lower and inter-band emission at higher HHG photon energies, the latter including the plateau and cutoff domain of the HHG spectrum.

Figure 1 presents a scheme of the basic mechanisms involved in the HHG process in pristine and doped MgO. Here, the Cr donor-dopants not only substitute Mg atoms with Cr^{3+} ions in the MgO lattice, providing additional electrons [see Figs. 1 (a) and 1 (b)], but also cause the formation of

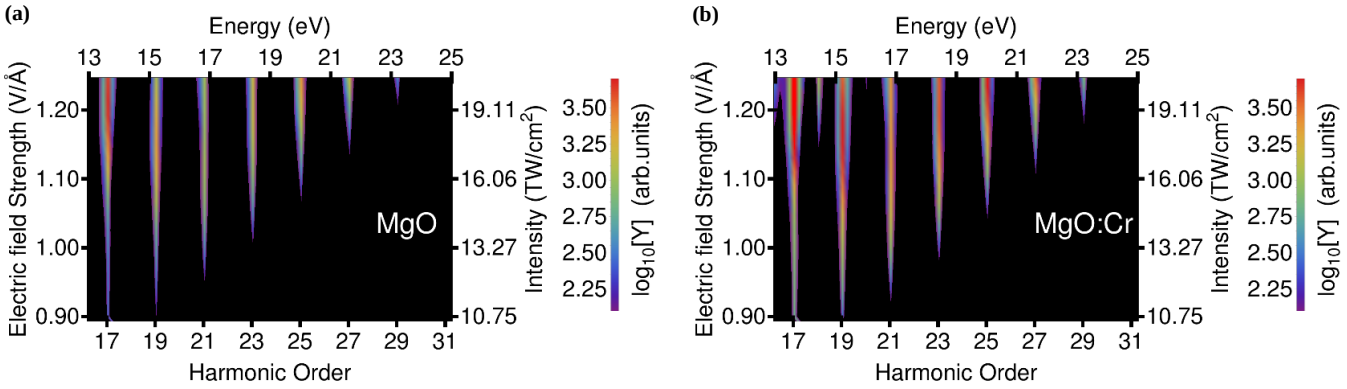

FIG. 2: Calculated HHG spectra from (a) MgO and (b) MgO:Cr crystals for driving laser-pulse incidence and HHG emission in $\Gamma - X$ direction as a function of the driver peak field strength. The laser central wavelength is 1.55 μm (corresponding to a photon energy of 0.80 eV, for details on the experimental parameters see SI.5.). Although the HHG yield from MgO:Cr is larger, we do not find evidence for a HHG cutoff extension for the doped sample.

vacancies[34–37] to maintain charge neutrality[37]. The underlying electronic excitations in pristine and Cr-doped MgO are sketched in Figs. 1 (c) and 1 (d), respectively. An electron wave packet is (1) excited from the valence band (VB) to the first conduction band (CB1) with an initial field-dressed crystal momentum at the minimum band gap (referred to as the $\Gamma-$point), where it (2) experiences intra-band acceleration. In case the laser electric field is strong enough, an electron wave packet is excited to a higher conduction band (CB2), where intra-band acceleration occurs, before (3) de-exciting to the VB upon recombination with its residual hole, emitting harmonics with photon energies equal to the instantaneous gap in the first BZ.

Within the Keldysh model for strong-field ionization[44] and a saddle-point analysis[45,46], a closed-form semi-quantitative approximation for the above band-gap (interband transition) yield is given by [47,48]

$$Y_{\mathrm{MgO}}(E) \propto \exp\left[-\frac{\sqrt{8m^*_{vb-cb1}}\,\varepsilon_g^{3/2}}{e\hbar E}\right], \qquad (1)$$

where $m^*_{vb-cb1} = \left(\left|\frac{1}{m^*_{vb}}\right| + \left|\frac{1}{m^*_{cb1}}\right|\right)^{-1}$ is the reduced effective mass of the VB and CB1, given in terms of their respective effective masses, m^*_{vb} and m^*_{cb1}, ε_g the minimum band-gap energy between VB and CB1, and E the peak field strength of the driving laser pulse. Similarly, we can account for excitations to higher conduction bands, e.g., to CB2 in our calculations, as sketched in Figs. 1 (c) and 1 (d), leading to the emission of harmonics at higher frequencies upon recombination to the VB. For a fixed driving electric-field amplitude, Eq. (1) predicts that a decrease of the minimum band gap or reduced effective mass increases the HHG spectral yield above the minimum band gap. Note that the effective electron mass is a crucial parameter responsible for the electron mobility in solids. Its energy-dependent behaviour was recently investigated[49,50]. Since the Cr impurities with associated vacancies break the transitional symmetry of the MgO crystal (in the BZ of the pristine crystal), impurity levels couple with states of the valence and conduction bands along the entire BZ. Together with the dispersion-free-electron nature of MgO impurity levels[29,51,52], which implies a very large effective mass, the loss of symmetry allows us to represent impurity levels as flat bands in the BZ of the pristine sample [shown as extended horizontal lines in Figs. 1 (c, d)]. The impurity-defect band (IDB) appears close to the CB1, and the vacancy defect band (VDB) emerges close to the VB. Adapting Eq. (1) to transitions from the VDB in MgO:Cr, we obtain the estimate for VDB contributions to the HHG yield

$$Y_{\mathrm{MgO:Cr}}(E) \propto \exp\left[-\frac{\sqrt{8m^*_{\text{vdb-cb1}}}\,(\varepsilon_{cb1}-\varepsilon_{vdb})^{3/2}}{e\hbar E}\right], \qquad (2)$$

where $m^*_{vdb-cb1}$ is the reduced effective mass between CB1 and VDB. Because of the large VDB effective mass, we can approximate $m^*_{vdb-cb1} \approx m^*_{cb1} > m^*_{vb-cb1}$. Thus, the reduced effective mass is greater than that for the pristine sample. Nevertheless, because of the reduction of the band gap induced by the vacancy, the numerator of the exponential in Eq. (2) is smaller than in Eq. (1), suggesting an enhancement of the HHG yield due to symmetry-allowed VDB - CB1 optical transitions.

For a fully quantitative description of HHG from pristine and doped MgO we numerically solve the semiconductor Bloch equations (SBEs), including the VB, IDB, CB1, and CB2 [for details see Supplementary Information (SI) SI.3.]. Disregarding temperature effects, the Fermi energy of MgO:Cr lies approximately between VDB and CB1[53], so that the VB and VDB are initially occupied.

Figure 2 (a, b) shows calculated HHG spectra from MgO and MgO:Cr, respectively. Both spectra are composed of odd harmonics (except for a dim even harmonic for the cal-

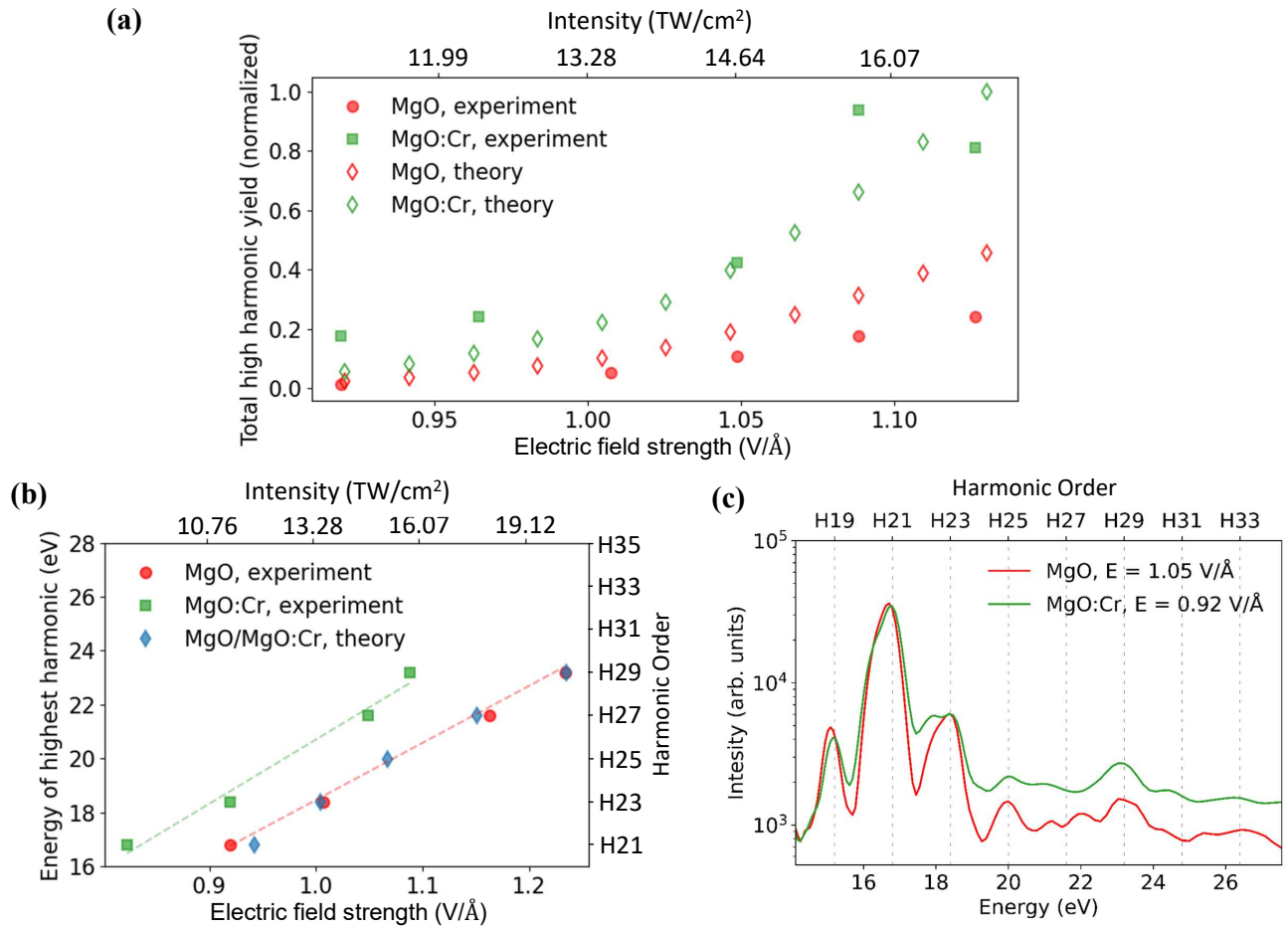

FIG. 3: Comparison of HHG signals from MgO and MgO:Cr crystals for a driving laser central wavelength of 1.55 μm (corresponding to a photon energy of 0.80 eV), (a) Measured and calculated total harmonic yields in the $\Gamma - X$ direction, integrated over photon energies between 14.4 and 25.6 eV, as a function of the peak driving laser-electric-field strength. The integrated HHG yield from MgO:Cr crystal is larger. (b) Highest observable harmonic energy versus the driving field strength in the $\Gamma - X$ direction. The offset of observed highest harmonic in both spectra is about 2 eV over a broad range of laser-electric-field strengths. It approximately matches the band-gap-energy difference between doped and undoped crystals. Dashed and solid lines are linear interpolations added to guide the eye. (c) Experimental HHG spectra obtained from MgO at a vacuum laser field strength of 1.05 V/Å (14.6 TW/cm^2) and from MgO:Cr at a vacuum laser field strength of 0.92 V/Å (11.2 TW/cm^2). In MgO:Cr a weaker laser electric field results in a comparable integrated HHG yield.

culated spectra from MgO:Cr) and exhibit almost the same field-strength dependence of the cutoff. The main difference between them is the increased inter-band harmonic spectral yield at above-band-gap photon energies for the material with vacancy defects. We analyze the HHG-yield enhancement by comparing the spectra in Figs. 2 (a, b) with our experimental data, estimating the intensity of the driving electric field inside the solids as detailed in the SI.7. Our laser field is sufficiently strong to excite electrons to the CB2, leading to the emission of harmonics in the XUV spectral range. Note that the consistent modeling of macroscopic optical effects, and the driving laser field strength in matter, would require merging our theoretical model with Maxwell's equations, which is beyond the scope of the current manuscript. Spectral transmission aspects are addressed in SI.2. The setup, intensity estimation, and the detailed description of the samples are given as SI. Both crystals, MgO and MgO:Cr, are 200-μm-thick with (001) oriented surfaces. We confirm the presence of Cr^{3+} ions in the MgO:Cr sample by photoluminescence measurements (SI.1.). In addition, the calculated densities of states (DOS) for MgO and MgO:Cr reveal defect states above the topmost valence band in MgO:Cr (SI.4.). Our transmission measurements show a band-gap-energy reduction of 1.8 eV in MgO:Cr, compared to the pure MgO band-gap energy of 7.16 eV (SI.2.).

Figure 3 (a) shows the dependence of the experimental harmonic yield, integrated between 14.4 and 25.6 eV, on the driving laser electric-field strength. The total HHG yield from MgO:Cr is found to be larger than the one of pure MgO,

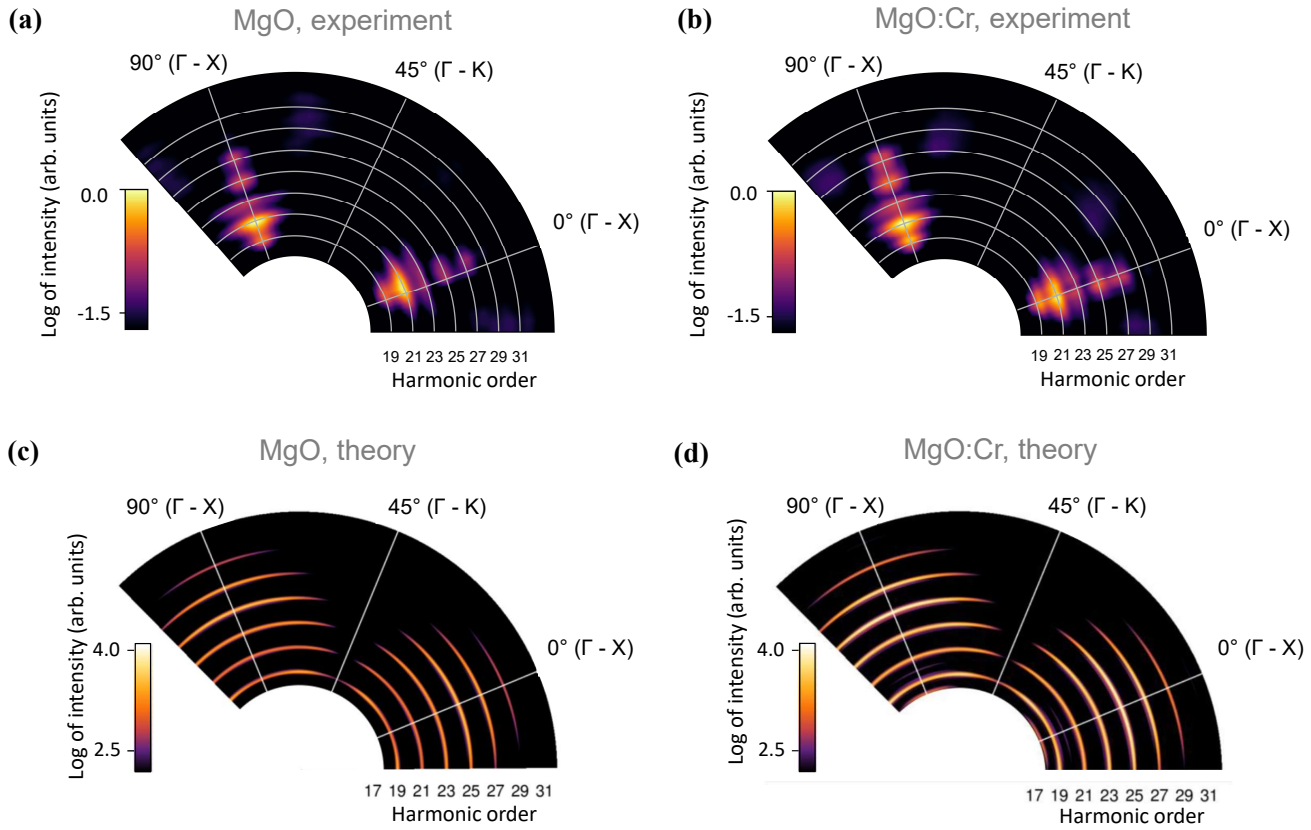

FIG. 4: Crystal-orientation dependence of HHG in (a,c) MgO and (b,d) MgO:Cr crystals. The crystals are rotated about the laser propagation axis [z axes in Figs. 1 (a) and 1 (b)] in 3-degree steps, while the linear laser polarization is kept fixed. Measured HHG spectra for (a) MgO at a peak laser-field strength (vacuum value) of 1.23 V/Å (20 TW/cm^2) and (b) MgO:Cr at 1.09 V/Å (15.7 TW/cm^2). Due to the low doping concentration (0.5%), the four-fold symmetry of the MgO cubic crystal structure is unaltered in MgO:Cr. Calculated spectra at 1.23 V/Å for (c) MgO and (d) MgO:Cr.

up to a laser-field strength of about 1.15 V/Å (corresponding to an intensity of 18 TW/cm^2). Operating at a repetition rate of 125 kHz, the damage threshold is reached at a laser electric-field strength of 1.23 V/Å (20 TW/cm^2) and 1.09 V/Å (15.7 TW/cm^2) for pure MgO and MgO:Cr, respectively. The lower damage threshold of MgO:Cr is probably associated with the increased electron density. In comparison, Fig. 3 (a) presents the numerically calculated intensities of odd harmonics for MgO and MgO:Cr, integrated over the same energy range. Our simulation results show good agreement with the experiment for pristine MgO and two discrepancies for doped MgO: (i) the experimental data show high harmonic emission starting at much lower laser-field strength, 0.71 V/Å (6.74 TW/cm^2), with a smaller slope than that obtained from the simulations based on solution of SBEs for doped MgO, (ii) the saturation of the HHG emission from MgO:Cr observed in the experiment is not reproduced by theory, since it involves mechanisms, such as radiation damage, which are not taken into account in the simulations. In spite of this, both, measured and calculated results exhibit a pronounced increase of the HHG spectral intensity from the MgO:Cr crystal, as the result of added transitions from the VDB.

Figure 3 (b) shows the highest harmonic order we are able to detect for driving-laser-field strengths (in vacuum) between 0.82 V/Å (9 TW/cm^2) and 1.23 V/Å (20 TW/cm^2) for both samples. It also shows HHG cutoffs retrieved from our calculated spectra in Fig. 2 (a, b). Figure 3 (b) shows a linear scaling of the highest experimentally detected harmonic as a function of the peak-electric-field strength in both MgO and MgO:Cr, with almost the same slope but an energy offset of approximately 2 eV. This energy offset is close to the band-gap-energy difference between MgO and MgO:Cr of ≈ 1.8 eV that we experimentally determined independently using optical transmission measurements (SI.1). The highest harmonic order obtained from the simulations in Figs. 2 (a), (b) is identical for MgO and MgO:Cr crystals. The extension of the highest experimentally observable harmonic from MgO:Cr is not

obvious. Indeed, since for the same electric-field strength the electron wave packet explores the same region of the first BZ of the MgO and MgO:Cr crystals, one might expect identical HHG cutoffs. We attribute the measured apparent extension of the HHG spectra from MgO:Cr to a higher yield in the plateau region. To further illustrate the HHG behavior, Fig. 3 (c) displays HHG spectra measured at a driving-laser peak field strength of 0.92 V/Å (11.2 TW/cm^2) for MgO:Cr and at 1.05 V/Å (14.6 TW/cm^2) for MgO. The two spectra have comparable yields even though the HHG spectrum from MgO:Cr was obtained at a lower laser field strength. This is in qualitative agreement with the simulated spectra displayed in Fig. 2. In addition, we notice in the experimental spectra that harmonics above 19 eV are less intense than those below this energy. This sharp transition between these two plateaus has been reported as contribution from higher conduction bands associated with low population transfer[54,55].

Moreover, we consider the contribution of macroscopic effects. The driving laser propagation inside the crystal can play a significant role on it's initial spatial or spectral properties and the emmited harmonic radiation[56]. Although the optical propagation effects related to the change of linear and nonlinear refractive indices due to doping are unlikely to play a significant role on the driving laser properties in our experiment, given the low dopant concentration of 0.5 %[57–60], we observe the difference of spatial and spectral properties of the harmonic beam from MgO and MgO:Cr. We detect a blueshift of the HHG spectra in MgO:Cr compared to HHG spectra from MgO at fixed laser intensity (SI.5.). We associate this wavelength shift to the increased electron density participating in HHG from MgO:Cr. Since the plasma refractive index variation acts as a diverging lens in the spatial domain, we attribute the observed blueshift to plasma-induced defocusing of the fundamental beam[61–63] (and references therein). Further investigations in a loose geometry configuration or in reflection geometry would limit possible contribution of macroscopic effects[56]. In a more general context, other crystals and/or higher doping rates may induce larger macroscopic aspects, that may play a significant role in enhancement or in spectral or spatial modifications of the HHG properties [19].

Next, we study the crystal-orientation dependent HHG response of both crystals. To investigate the HHG anisotropy, we measure the HHG signal as a function of the crystal orientation with respect to the laser polarization, as sketched in Fig. 1 (a, b) and described in SI.5. Figures 4 (a) and 4 (b) present angle-dependent measured HHG spectra from MgO and MgO:Cr, recorded at their respective optimal conditions for highest HHG yields, i.e., just below the damage threshold at peak electric-field strengths of 1.23 V/Å (20 TW/cm^2) for MgO and 1.09 V/Å (15.7 TW/cm^2) for MgO:Cr. The fourfold symmetry reflects the face-centered cubic crystal structure of MgO[64]. The HHG yield is largest along the $\Gamma - X$ direction while no signal is observed along the $\Gamma - K$ direction. Overall, the two anisotropy dependences are comparable, which is consistent with the fact that the crystal symmetry is preserved for our low dopant concentrations. We observe that, similar to Fig. 3 (a), the harmonics emitted from MgO:Cr have a comparable yield at a lower driving-field intensities than harmonics from pure MgO. To analyze this behavior, we have calculated the angle-dependent HHG yield for MgO and MgO:Cr at the same peak vacuum electric-field strength of 1.23 V/Å (20 TW/cm^2), as shown in Figs. 4 (c) and 4 (d). These calculations are performed in reduced dimensionality, representing the crystal as a 2D square lattice using the same model electronic potential as in recent works,[2,65,66] $V(x,y) = V_0\cos(ax) + V_0\cos(ay)$, but allowing for a modified oscillation amplitude V_0 at the defect sites in MgO:Cr[30,31,33,67,68] (SI.3.). Even though the angular spread of the harmonics differs between theory and experiment, we reproduce the maximal yields measured along the $\Gamma - X$ and the minimal yields along the $\Gamma - K$ direction. For all crystal orientations our numerical simulation predicts a larger HHG yield for MgO:Cr. These two last characteristics are in good qualitative agreement with the present experimental findings.

In conclusion, we present the HHG yield enhancement from MgO doped with chromium atoms compared to pure a MgO crystal. We associate the extension of the highest observable harmonic in MgO:Cr to an increase of the HHG plateau intensity. The HHG yield increase from the doped crystal is interpreted as optical excitations introduced by occupied defect states in MgO:Cr that arise from Cr^{3+} dopant ions and Mg-vacancy formation in the MgO lattice. This finding is in agreement with our numerical simulations and previous theoretical predictions of enhanced HHG in doped samples[30,31,33,67]. The HHG anisotropy shows that the pristine MgO crystal symmetry is preserved upon doping. Our numerical results do not reproduce the experimentally observed HHG spectral blue shift and saturation, both caused by additional free electrons in the doped MgO, which we attribute to our incomplete description of the driving laser pulse in the solid. Other crystals involved in the HHG or other dopant concentrations may enchance macroscopic effects that could be exploited to boost the HH yield in specific spectral ranges. As a perspective, our study promotes the development of efficient compact XUV light sources based on doping. Moreover, it has been suggested that HHG from crystals with defects can provide a way to study dipole moments and wave functions of impurity arrangements[68] and thus potentially serve as a tomographic measurement of impurity orbitals. Other future studies will concentrate on HHG spectroscopy to extract information on the intrinsic properties of light-driven attosecond electron transport[69]. This would create attractive perspectives towards the development of all-solid-state attosecond sources and petahertz electronics[12–14,29–33,55].

ACKNOWLEDGMENTS

Authors thank M. Billon for technical support. We acknowledge support from the PETACom (Petahertz Optoelectronics Communication) FET Open H2020 grant number 829153, OPTOLogic (Optical Topologic Logic) FET Open H2020 grant number 899794, support from the French ANR through the grant PACHA (ANR-17-CE30-0008-01) and the labex PALM (ANR-10-LABX-0039- PALM), support the DGA RAPID grant "SWIM". We acknowledge the

financial support from the French ASTRE program through the "NanoLight" grant, the Spanish Ministry MINECO (National Plan 15 Grant: FISICATEAMO No. FIS2016-79508-P, SEVERO OCHOA No. SEV-2015-0522, FPI), European Social Fund, Fundació Cellex, Fundació Mir-Puig, Generalitat de Catalunya (AGAUR Grant No. 2017 SGR 1341, CERCA/Program), ERC AdG NOQIA, EU FEDER, European Union Regional Development Fund - ERDF Operational Program of Catalonia 2014-2020 (Operation Code: IU16-011424), MINECO-EU QUANTERA MAQS (funded by The State Research Agency (AEI) PCI2019-111828-2/10.13039/501100011033), and the National Science Centre, Poland-Symfonia Grant No. 2016/20/W/ST4/00314. F. N. and U. T. acknowledge support from Air Force Office of Scientific Research under award number FA9550-17-1-0369 and NSF Grant No. 1802085 (theory for photoemission from surfaces). N. T.-D. thanks A. Rubio.

DATA AVAILABILITY

The data that support the findings of this study are available within the article and its supplementary material.

REFERENCES

[1] S. Ghimire, A. D. DiChiara, E. Sistrunk, G. Ndabashimiye, U. B. Szafruga, A. Mohammad, P. Agostini, L. F. DiMauro, and D. A. Reis, "Generation and propagation of high-order harmonics in crystals," Phys. Rev. A **85**, 043836 (2012).

[2] G. Vampa, C. R. McDonald, G. Orlando, D. D. Klug, P. B. Corkum, and T. Brabec, "Theoretical analysis of high-harmonic generation in solids," Phys. Rev. Lett. **113**, 073901 (2014).

[3] T. T. Luu and H. J. Wörner, "High-order harmonic generation in solids: A unifying approach," Phys. Rev. B **94**, 115164 (2016).

[4] N. Tancogne-Dejean, O. D. Mücke, F. X. Kärtner, and A. Rubio, "Impact of the electronic band structure in high-harmonic generation spectra of solids," Phys. Rev. Lett. **118**, 087403 (2017).

[5] S. Ghimire, A. D. DiChiara, E. Sistrunk, P. Agostini, L. F. DiMauro, and D. A. Reis, "Observation of high-order harmonic generation in a bulk crystal," Nature Physics **7**, 138 (2011).

[6] G. Vampa, C. McDonald, A. Fraser, and T. Brabec, "High-harmonic generation in solids: bridging the gap between attosecond science and condensed matter physics," IEEE Journal of Selected Topics in Quantum Electronics **21**, 8700110 (2015).

[7] M. Garg, M. Zhan, T. T. Luu, H. Lakhotia, T. Klostermann, A. Guggenmos, and E. Goulielmakis, "Multi-petahertz electronic metrology," Nature **538**, 359 (2016).

[8] H. Kim, S. Han, Y. W. Kim, S. Kim, and S.-W. Kim, "Generation of coherent extreme-ultraviolet radiation from bulk sapphire crystal," ACS Photonics **4**, 1627 (2017).

[9] D. Franz, S. Kaassamani, D. Gauthier, R. Nicolas, M. Kholodtsova, L. Douillard, J.-T. Gomes, L. Lavoute, D. Gaponov, N. Ducros, S. Février, J. Biegert, L. Shi, M. Kovačev, W. Boutu, and H. Merdji, "All semiconductor enhanced high-harmonic generation from a single nanostructured cone," Scientific Reports **9**, 5663 (2019).

[10] D. Gauthier, S. Kaassamani, D. Franz, R. Nicolas, J.-T. Gomes, L. Lavoute, D. Gaponov, S. Février, G. Jargot, M. Hanna, W. Boutu, and H. Merdji, "Orbital angular momentum from semiconductor high-order harmonics," Optics Letters **44**, 546 (2019).

[11] A. A. Lanin, E. A. Stepanov, A. B. Fedotov, and A. M. Zheltikov, "Mapping the electron band structure by intraband high-harmonic generation in solids," Optica **4**, 516 (2017).

[12] F. Krausz and M. I. Stockman, "Attosecond metrology: from electron capture to future signal processing," Nature Photonics **8**, 205 (2014).

[13] J. Schoetz, Z. Wang, E. Pisanty, M. Lewenstein, M. F. Kling, and M. F. Ciappina, "Perspective on petahertz electronics and attosecond nanoscopy," ACS Photonics **6**, 3057 (2019).

[14] S. Sederberg, D. Zimin, S. Keiber, F. Siegrist, M. S. Wismer, V. S. Yakovlev, I. Floss, C. Lemell, J. Burgdörfer, M. Schultze, F. Krausz, and N. Karpowicz, "Attosecond optoelectronic field measurement in solids," Nature Communications **11**, 1 (2020).

[15] R. E. F. Silva, A. Jiménez-Galán, B. Amorim, O. Smirnova, and M. Ivanov, "Topological strong-field physics on sub-laser-cycle timescale," Nature Photonics **13**, 849 (2019).

[16] S. Han, H. Kim, Y.-W. Kim, Y.-J. Kim, S. Kim, I.-Y. Park, and S.-W. Kim, "High-harmonic generation by field enhanced femtosecond pulses in metal-sapphire nanostructure," Nature Communications **7**, 13105 (2016).

[17] G. Vampa, B. G. Ghamsari, S. Siadat Mousavi, T. J. Hammond, A. Olivieri, E. Lisicka-Skrek, A. Y. Naumov, D. M. Villeneuve, A. Staudte, P. Berini, and P. B. Corkum, "Plasmon-enhanced high-harmonic generation from silicon," Nature Physics **13**, 659 (2017).

[18] D. Franz, R. Nicolas, W. Boutu, L. Shi, , Q. Ripault, M. Kholodtsova, B. Iwan, U. E. Etxano, M. Kovacev, J. Biegert, and H. Merdji, "Amplification of high harmonics in 3d semiconductor waveguides," arXiv **09153v1** (2017).

[19] M. Sivis, M. Taucer, G. Vampa, K. Johnston, A. Staudte, A. Naumov, D. Villeneuve, C. Ropers, and P. Corkum, "Tailored semiconductors for high-harmonic optoelectronics," Science **357**, 303 (2017).

[20] K. Imasaka, T. Kaji, T. Shimura, and S. Ashihara, "Antenna-enhanced high harmonic generation in a wide-bandgap semiconductor ZnO," Optics Express **26**, 21364 (2018).

[21] T. Umebayashi, T. Yamaki, H. Itoh, and K. Asai, "Band gap narrowing of titanium dioxide by sulfur doping," Appl. Phys. Lett. **81**, 454 (2002).

[22] N. Kamarulzaman, M. F. Kasim, and N. F. Chayed, "Elucidation of the highest valence band and lowest conduction band shifts using XPS for ZnO and $Zn_{0.99}Cu_{0.01}O$ band gap changes," Results in Physics **6**, 217 (2016).

[23] D. Auvergne, J. Camassel, and H. Mathieu, "Band-gap shrinkage of semiconductors," Phys. Rev. B **11**, 2251 (1975).

[24] H. J. Queisser and E. E. Haller, "Defects in semiconductors: some fatal, some vital," Science **281**, 945 (1998).

[25] F. Oba and Y. Kumagai, "Design and exploration of semiconductors from first principles: A review of recent advances," Appl. Phys. Express **11**, 060101 (2018).

[26] C. Di Valentin and G. Pacchioni, "Spectroscopic properties of doped and defective semiconducting oxides from hybrid density functional calculations," Accounts of chemical research **47**, 3233 (2014).

[27] B. Henderson and G. F. Imbusch, "Optical spectroscopy of inorganic solids," Oxford University Press **23**, 2824 (1989).

[28] A. V. Chadwick and M. Terenzi, "Defects in solids: modern techniques," Springer Science & Business Media **23**, 2824 (2013).

[29] M. S. Mrudul, N. Tancogne-Dejean, A. Rubio, and G. Dixit, "High-harmonic generation from spin-polarised defects in solids," Npj Computational Materials **6**, 10 (2020).

[30] T. Huang, X. Zhu, L. Li, X. Liu, P. Lan, and P. Lu, "High-order-harmonic generation of a doped semiconductor," Phys. Rev. A **96**, 043425 (2017).

[31] C. Yu, K. K. Hansen, and L. B. Madsen, "Enhanced high-order harmonic generation in donor-doped band-gap materials," Phys. Rev. A **99**, 013435 (2019).

[32] X.-F. Pan, T. Han, C.-L. Xia, T.-T. Xu, J. Zhang, and X.-S. Liu, "Energy band splitting and high-order harmonic generation from a doped semiconductor," Laser Phys. Lett. **16**, 115301 (2019).

[33] H. Iravani, K. K. Hansen, and L. B. Madsen, "Effects of vacancies on high-order harmonic generation in a linear chain with band gap," Phys. Rev. Research **2**, 013204 (2020).

[34] M. O. Henry, J. P. Larkin, and G. F. Imbusch, "Nature of the broadband luminescence center in MgO:Cr^{3+}," Phys. Rev. B **13**, 1893 (1976).

[35] J. B. Wachtman and A. D. E. Franklin, "Mass transport in oxides," Proceedings of a symposium held at Gaithersburg, Maryland, October 22-25, 1967 **13**, 12 (1968).

[36] F. Stavale, N. Nilius, and H.-J. Freund, "Cathodoluminescence of near-surface centres in Cr-doped MgO(001) thin films probed by scanning tunnelling microscopy," New Journal of Physics **14**, 033006 (2012).

[37] E. Shablonin, A. I. Popov, A. Lushchik, A. Kotlov, and S. Dolgova, "Excitation of different chromium centres by synchrotron radiation in MgO:Cr single crystals," Physica B: Condensed Matter **477**, 133 (2015).

[38] J. Aramburu, P. García-Fernández, M. Barriuso, and M. Moreno, "Transition metal complexes coupled to vacancies in oxides: Origin of different properties of Cr^{3+} in MgO bounded to a <100> or <110> Mg^{2+} vacancy," The Journal of Physical Chemistry A **117**, 12642 (2013).

[39] J. Aramburu, P. Garcia-Fernandez, J. Garcia-Lastra, M. Barriuso, and M. Moreno, "Colour due to Cr^{3+} ions in oxides: a study of the model system MgO:Cr^{3+}," Journal of Physics: Condensed Matter **25**, 175501 (2013).

[40] M. Novita and K. Ogasawara, "Study on multiplet energies of V^{2+}, Cr^{3+}, and Mn^{4+} in MgO host crystal based on first-principles calculations with consideration of lattice relaxation," Journal of the Physical Society of Japan **83**, 124707 (2014).

[41] J. L. Krause, K. J. Schafer, and K. C. Kulander, "High-order harmonic generation from atoms and ions in the high intensity regime," Phys. Rev. Lett. **68**, 3535 (1992).

[42] P. B. Corkum, "Plasma perspective on strong field multiphoton ionization," Phys. Rev. Lett. **71**, 1994 (1993).

[43] K. C. Kulander, K. J. Schafer, and K. L. Krause, "Super-intense laser-atom physics," Vol. 316 of NATO Advanced Study Institute Series B: Physics, Plenum, New York **68**, 95 (1993).

[44] L. V. Keldysh, "Ionization in the field of a strong electromagnetic wave," Sov. Phys. JETP **20**, 1307 (1965).

[45] M. Lewenstein, P. Balcou, M. Y. Ivanov, A. L'Huillier, and P. B. Corkum, "Theory of high-harmonic generation by low-frequency laser fields," Phys. Rev. A **49**, 2117 (1994).

[46] R. Wong, "Asymptotic approximations of integrals," Society for Industrial and Applied Mathematics **34** (2001).

[47] F. Navarrete, M. F. Ciappina, and U. Thumm, "Crystal-momentum-resolved contributions to high-order harmonic generation in solids," Phys. Rev. A **100**, 033405 (2019).

[48] F. Navarrete and U. Thumm, "Two-color-driven enhanced high-order harmonic generation in solids," Phys. Rev. A **102**, 063123 (2020).

[49] L. Kasmi, M. Lucchini, L. Castiglioni, P. Kliuiev, J. Osterwalder, M. Hengsberger, L. Gallmann, P. Krüger, and U. Keller, "Effective mass effect in attosecond electron transport," Optica **4**, 1492 (2017).

[50] M. J. Ambrosio and U. Thumm, "Spatiotemporal analysis of a final-state shape resonance in interferometric photoemission from Cu(111) surfaces," Phys. Rev. A **100**, 043412 (2019).

[51] P. V. C. Medeiros, S. Stafström, and J. Björk, "Effects of extrinsic and intrinsic perturbations on the electronic structure of graphene: Retaining an effective primitive cell band structure by band unfolding," Phys. Rev. B **89**, 041407 (2014).

[52] M. Hjort and S. Stafström, "Modeling vacancies in graphite via the Hückel method," Phys. Rev. B **61**, 14089 (2000).

[53] C. Kittel, *Quantum Theory of Solids* (Wiley, 1987).

[54] A. J. Uzan, G. Orenstein, A. Jiménez-Galán, C. McDonald, R. E. F. Silva, B. D. Bruner, N. D. Klimkin, V. Blanchet, T. Arusi-Parpar, M. Krüger, A. N. Rubtsov, O. Smirnova, M. Ivanov, B. Yan, T. Brabec, and N. Dudovich, "Attosecond spectral singularities in solid-state high-harmonic generation," Nature Photonics **14**, 183 (2020).

[55] Y. S. You, M. Wu, Y. Yin, A. Chew, X. Ren, S. Gholam-Mirzaei, D. A. Browne, M. Chini, Z. Chang, K. J. Schafer, M. B. Gaarde, and S. Ghimire, "Laser waveform control of extreme ultraviolet high harmonics from solids," Optics Letters **42**, 1816 (2017).

[56] G. Vampa, Y. S. You, H. Liu, S. Ghimire, and D. A. Reis, "Observation of backward high-harmonic emission from solids," Optics Express **26**, 12210 (2018).

[57] A. Miller and D. Finlayson, "Laser sources and applications," CRC Press , 315 (1997).

[58] M. Lai, J. Nicholson, and W. Rudolph, "Multiple pulse operation of a femtosecond Ti:sapphire laser," Optics communications **142**, 45 (1997).

[59] J. Philip, C. D'Amico, G. Cheriaux, A. Couairon, B. Prade, and A. Mysyrowicz, "Amplification of femtosecond laser filaments in Ti:Sapphire," Phys. Rev. Lett. **95**, 163901 (2005).

[60] Y. Guo, S. Lu, L. Su, C. Zhao, H. Zhang, and S. Wen, "Z-scan measurement of the nonlinear refractive index of Nd^{3+}, Y^{3+}-codoped CaF_2 and SrF_2 crystals," Applied Optics **54**, 953 (2015).

[61] S. C. Rae, "Spectral blueshifting and spatial defocusing of intense laser pulses in dense gases," Optics communications **104**, 330 (1994).

[62] A. Heins, S. C. Singh, and C. Guo, "Electron kinetic energy and plasma emission diagnosis from femtosecond laser produced air plasmas," Physics of Plasmas **24**, 072101 (2017).

[63] V. E. Nefedova, M. F. Ciappina, O. Finke, M. Albrecht, J. Vábek, M. Kozlová, N. Suárez, E. Pisanty, M. Lewenstein, and J. Nejdl, "Determination of the spectral variation origin in high-order harmonic generation in noble gases," Phys. Rev. A **98**, 033414 (2018).

[64] Y. S. You, D. Reis, and S. Ghimire, "Anisotropic high-harmonic generation in bulk crystals," Nature Physics **13**, 345 (2017).

[65] M. Wu, S. Ghimire, D. A. Reis, K. J. Schafer, and M. B. Gaarde, "High-harmonic generation from bloch electrons in solids," Phys. Rev. A **91**, 043839 (2015).

[66] X. Liu, X. Zhu, P. Lan, X. Zhang, D. Wang, Q. Zhang, and P. Lu, "Time-dependent population imaging for high-order-harmonic generation in solids," Phys. Rev. A **95**, 063419 (2017).

[67] A. Pattanayak, M. M. S., and G. Dixit, "Influence of vacancy defects in solid high-order harmonic generation," Phys. Rev. A **101**, 013404 (2020).

[68] S. Almalki, A. M. Parks, G. Bart, P. B. Corkum, T. Brabec, and C. R. McDonald, "High harmonic generation tomography of impurities in solids: Conceptual analysis," Phys. Rev. B **98**, 144307 (2018).

[69] Q. Liao, W. Cao, Q. Zhang, K. Liu, F. Wang, P. Lu, and U. Thumm, "Distinction of electron dispersion in time-resolved photoemission spectroscopy," Phys. Rev. Lett. **125**, 043201 (2020).